https://doi.org/10.5194/egusphere-2026-899
Preprint. Discussion started: 24 February 2026

Simulation of climate during the Miocene Climatic Optimum under different CO_2 forcings

Hamida Ngoma Nadoya[1], Clay R. Tabor[1], Ran Feng[1], Xiaoqing Liu[2], Daniel E. Ibarra[3], Tammo Reichgelt[1], Amber Laskos[1]

[1]Department of Earth Sciences, University of Connecticut, Storrs, CT, USA
[2] Department of Earth, Atmospheric and Planetary Sciences, Purdue University, West Lafayette, IN, USA
[3]Department of Earth, Environmental and Planetary Sciences, Providence, RI, USA
Correspondence to: Nadoya, H.N (hamida.nadoya@uconn.edu)

Abstract:
The Miocene Climatic Optimum (MCO; 17 – 14 Ma), characterized by global mean surface temperatures ~7°C higher than preindustrial (PI), offers a target for validating models for warmer-than-present climate states. Here, we use a water isotope tracer enabled version of the Community Earth System Model to simulate the MCO under 1x (MCO1x), 2x (MCO2x), and 4x (MCO4x) PI CO_2. Our simulations show significant warming due to MCO boundary conditions as well as a small increase in equilibrium climate sensitivity with higher CO_2. All simulations exhibit a decreased mean equator-to-pole temperature gradient relative to PI. However, the spatial patterns of warming are distinct between simulations with relatively greater high latitude warming between MCO1x and MCO2x and relatively greater low latitude warming between MCO2x and MCO4x. Warming is associated with enhanced precipitation and enriched precipitation $\delta^{18}O$ ($\delta^{18}O_p$) globally.

We compare the MCO model outputs with proxy of surface temperature, precipitation, and $\delta^{18}O_p$. Like many other MCO modeling studies, our simulations underestimate the reduced latitudinal temperature gradient reconstructed with proxies. We find better model-proxy agreement for terrestrial and marine temperature records in the MCO1x and MCO4x experiments, respectively. Precipitation and $\delta^{18}O_p$ records show the best agreement with the MCO2x and MCO1x experiments, respectively, but there are large uncertainties due to limited proxy data and large reconstruction uncertainties. The MCO2x simulation is warmer than the projected 2080-2100 climate under RCP8.5, highlighting the importance of both boundary conditions and equilibrium versus transient climate system response to increased CO_2.

1 Introduction

Many studies linking past warm climates to the future have focused on the mid-Pliocene Warm Period with CO_2 of ~400 ppm (e.g. Haywood et al., 2020) and the Early Eocene Climatic Optimum with CO_2 likely >1000 ppm (e.g. Lunt et al., 2021). However, mid-Pliocene atmospheric CO_2 concentrations have already been surpassed, and ongoing mitigation efforts make it unlikely that CO_2 concentrations greater than the Early Eocene Climatic Optimum will be reached by 2100. Consequently, the Miocene Climate Optimum (MCO; 17 – 14 Ma), which likely featured CO_2 concentrations between 2x and 4x preindustrial (Hönisch et al., 2023), is now a valuable interval for understanding climate change under more plausible future scenarios.

The MCO, ~7°C warmer than PI, was characterized by a reduced equator to pole temperature gradient and poleward-shifted bioclimatic zones (Steinthorsdottir et al., 2021). Proxy reconstructions suggest that sea surface temperatures (SSTs) were 10 – 15°C warmer in the northern high-latitudes (~above 42°N; Super et al., 2020) and 8 – 10°C warmer in the southern

https://doi.org/10.5194/egusphere-2026-899
Preprint. Discussion started: 24 February 2026

high-latitudes (Tasmanian Gateway; Shevenell et al., 2008). Over land, northern hemisphere (NH) high-latitudes warmed by 5 – 14°C and experienced increased precipitation (Pound et al., 2012; Reichgelt and West, 2025). Relatedly, vegetation reconstructions reveal heavily forested areas extended over the Arctic and tundra covered parts of Antarctica (Bradshaw et al., 2025) while the mid-latitudes were more forested than they are today (Reichgelt and West, 2025). Furthermore, the MCO was characterized by sea ice-free northern hemisphere summers and sea level rise of ~48 m relative to PI (Gasson et al., 2016; Steinthorsdottir et al., 2021).

MCO CO_2 reconstructions remain uncertain. Early estimates suggested CO_2 levels of less than 500 ppm (Zhang et al., 2013; Greenop et al., 2014). However, MCO simulations with CO_2 levels less than 500 ppm underestimate proxy-reconstructed warming, the equator-to-pole temperature gradient, and precipitation (Burls et al., 2021). More recently, boron isotope-based estimates suggest CO_2 as high as 4-times PI (Rae et al., 2021; Hönisch et al., 2023). With higher prescribed CO_2, MCO simulations tend to better agree with high-latitude temperatures from proxy reconstructions but may overestimate tropical surface temperatures; the magnitude varies between models (Burls et al., 2021).

Some more recent Earth system models have a higher equilibrium climate sensitivity, which may make them better at simulating MCO warmth with lower CO_2 concentrations. However, few of these higher equilibrium climate sensitivity models have been run with MCO boundary conditions. Furthermore, most previous simulations of the MCO did not incorporate water isotope tracers, which limited model-proxy comparisons.

In this study, to bridge the model-proxy gap we use a fully-coupled, water isotope tracer enabled Earth system model run with MCO boundary conditions. Our chosen Earth system model has a moderately high equilibrium climate sensitivity and has shown to be one of the best performing models for simulation of the Eocene (Zhu et al., 2019) and Pliocene (Feng et al., 2020). Furthermore, it has been found to reliably simulate the oxygen isotopic composition of precipitation in the past and present (Zhu et al., 2017; Brady et al., 2019). We ran three CO_2 scenarios, 1x, 2x, and 4x PI, to test the effect of atmospheric CO_2 on Miocene climate and directly compare with proxy records to minimize model-proxy biases.

2 Data and methodology

2.1 Model and experiments

We use the water isotope tracer enabled Community Earth System Model version 1.2 (iCESM1.2; Brady et al., 2019). iCESM1.2 is a fully coupled Earth system model and can simulate the movement of stable oxygen and hydrogen isotopes through atmosphere, land, ocean, sea ice, and river transport components. Here, the atmosphere component is the Community Atmosphere Model version 5 with the Modal Aerosol Model (CAM5-MAM3; Neale et al., 2010) and the land component is the Community Land Model version 4 with carbon and nitrogen cycling (CLM4-CN; Oleson et al., 2010). We use the finite volume dynamical core with a resolution of 1.9° × 2.5° latitude / longitude. The atmosphere has 30 vertical levels. The ocean component is the Parallel Ocean Program version 2 (POP2; Smith et al., 2010), and the sea ice component is the Los Alamos Sea Ice Model version 4 (CICE4; Hunke, 2010). The ocean grid has 320 x 394 cells with a nominal resolution of 1° and 60 levels in the vertical. Following Feng et al. (2020), 10 extra rows were added to the default ocean grid in order to simulate the deglaciated western Antarctic.

Boundary conditions of topography, bathymetry, vegetation, and land ice cover come from the mid-Miocene reconstruction by Frigola et al. (2018). For this study, we raised the Andes following Boschman (2021), who suggested a high central Andes during the MCO based on stable isotopic composition of carbonates and volcanic ash. Using these boundary conditions, we

https://doi.org/10.5194/egusphere-2026-899
Preprint. Discussion started: 24 February 2026

performed three MCO experiments with CO_2 of 1x (284.7 ppm; MCO1x), 2x (569.4 ppm; MCO2x), and 4x (1138.8 ppm; MCO4x) PI level. All other greenhouse gases as well as orbital parameters were set to the default PI values in CESM1 (Hurrell et al., 2013).

The MCO2x case was integrated for 4,050 years to attain an equilibrium climate state with a net top of atmosphere (TOA) energy imbalance of -0.04 W/m^2. The MCO1x and MCO4x simulations were initialized from the MCO2x simulation after running it for 2,500 years. For the MCO4x simulation, ocean temperatures were initially increased by 4.5°C to speed up the equilibrium process. The MCO1x experiment was run for 2,850 years and the MCO4x experiment for 2,000 years, reaching near-equilibrium states with net TOA energy imbalances of 0.03 and -0.09 W/m^2, respectively. A preindustrial simulation was also run for 300 years, starting from the default PI initial conditions. Here, we analyze and present the last 100 years of the simulations.

2.2 Proxy data

Proxy data from published literature are compared with the model outputs. This includes temperature and precipitation reconstructions as well as oxygen isotope data. Proxy temperature reconstructions are adapted from the compilation in Burls et al. (2021) and other published literature and cover the period from 16.75 to 14.5 Ma. The compilation consists of SST reconstructions based on U^K_{37} (Brassel, 2014), Mg/Ca (Holland et al., 2020; Hollis et al., 2019), and TEX_{86} (Schouten et al., 2002). The proxy techniques used for comparison pose some challenges and caution needs to be taken when interpreting the proxies for different regions. For example, the use of U^K_{37}, in the tropics is limited during the MCO as the proxy reaches a thermal limit under very warm conditions (Tierney et al., 2018). Furthermore, TEX_{86} may be influenced by temperature signals below the surface mixed layer (Lopes dos Santos et al., 2010) and have a seasonal bias (Jia et al., 2017). Mg/Ca also has uncertainties associated with ocean pH, salinity, and Mg/Ca (Gray and Evans, 2019). Terrestrial temperature reconstructions are updated from compilations in Pound et al. (2012) and Goldner et al. (2014) as well as geochemical reconstructions based on the distribution of branched tetraethers in sediments from plant fossils (Weijers et al., 2009). The plant fossil reconstructions employ one of three approaches: co-existence (Utescher et al., 2014), Climate Leaf Analysis Multivariate Program (CLAMP; Spicer at al., 2021; Gibson et al., 2022), and Leaf Margin Analysis (LMA; Uhl et al., 2003). Precipitation data comes from the compilation in Herold et al (2011) and other published literature (Acosta et al., 2024; Pound et al., 2012; Bradshaw et al., 2012, Reichgelt and West, 2025, SP Table 1). The precipitation data were reconstructed from plant fossils following either the co-existence approach (Utescher et al., 2014) or CLAMP (Spicer at al., 2021; Gibson et al., 2022). $\delta^{18}O$ values are sourced from the Paleo Analysis of Terrestrial Climate and Hydrology (PATCH) Lab database (Kukla et al., 2022). The data includes measurements from inorganic carbonates, mammalian teeth, phyllosilicate, and shells. In addition, the sample minerals include calcite, alunite, dolomite, apatite, aragonite, smectite, and chert. The data were calibrated to precipitation $\delta^{18}O$ values in VSMOW assuming equilibrium precipitation for formation temperature depending on the mineral type i.e calcite (Kim and O'Neil, 1997), alunite (Rye and Stoffregen, 1995), dolomite (Land, 1983), apatite (Longinelli & Nuti, 1973; Kolodny et al., 1983), aragonite (Grossman and Ku, 1986), smectite (Savin and Lee, 1988), and chert (Knauth and Esptein, 1976).

2.3 Future climate projections

We also compare our MCO simulations with future climate projections. Since our MCO simulations use CESM1, we compared them with future simulations from CESM1. CESM1 has

https://doi.org/10.5194/egusphere-2026-899
Preprint. Discussion started: 24 February 2026

not been used to simulate the Shared Socioeconomic Pathway (SSP; Riahi et al., 2017) scenarios. We therefore chose to use Representative Concentration Pathways (RCP) data from the Coupled Model Intercomparison Project Phase five (CMIP5; Taylor et al., 2012). We use the CESM1 Large Ensemble (Kay et al., 2015) under RCP8.5 considering the ensemble mean of the first five realizations. Atmospheric CO_2 concentrations under RCP8.5 scenario reach 1000 ppm by the end of the century (IPCC, 2013, 2017, 2021).

2.4 Energy Balance Model

To assess the drivers of the surface temperature responses, we use a 1-dimensional energy balance model to decompose the simulated zonal-mean annual surface temperature changes between the three MCO simulations into contributions from emissivity, albedo, and meridional heat convergence (Lunt et al., 2012; Hill et al., 2014). We use the Approximate Partial Radiative Perturbation (APRP) technique to further separate planetary albedo changes into changes due to surface, clear sky, and clouds (Taylor et al., 2007; Feng et al., 2017). APRP helps separate cloud albedo and surface albedo changes, which are particularly challenging in the polar regions where effects due to surface reflection can be mistaken as effects due to cloud reflection.

3 Results

3.1 Mean climate and response to atmospheric CO_2

3.1.1 Surface Temperature

Our results show global mean annual surface temperatures (MAT) of 18.4, 22.3, 26.4°C in the MCO1x, MCO2x, and MCO4x cases, respectively (Table 1). Meridional temperature gradients between the tropics (15°S – 15°N) and high-latitudes (>60° N/S) of 37.5, 29.3, and 25.7°C are observed for the northern hemisphere (NH) and 41.7, 37.8, and 34.5°C for the southern hemisphere (SH). In the MCO1x experiment, high-latitude (>60° N/S) mean surface temperatures are -8.8°C in the NH and -13.3°C in the SH (Fig. 1); midlatitude (30–60°N/S) mean surface temperatures are 11.4°C in the NH and 15.6°C in the SH; tropical (15°S–15°N) mean surface temperatures are 28.7°C. Warmest surface temperatures >32°C are observed over the equatorial Pacific, Indian, and South Atlantic Oceans. Over land, warmest temperatures are observed over India and parts of the Sahara. Surface temperature climatologies for the 2x and 4x MCO experiments can be found in the supplemental information (Fig. SP3).

The doubling of CO_2 results in an equilibrium climate sensitivity of 3.9°C from 1x to 2x PI CO_2 and 4.1°C from 2x to 4x PI CO_2 (Fig. 1d). In addition, increasing CO_2 from 1x to 2x PI CO_2 results in high-latitude warming of 10.9°C in the NH and 6.6°C in the SH, while increasing CO_2 from 2x to 4x PI CO_2 results in warming of 6.8°C in the NH and 6.5°C in the SH. In the midlatitudes, increasing CO_2 from 1x to 2x PI CO_2 results in warming of 5.5°C in the NH and 2.7°C in the SH and from 2x to 4x PI CO_2 results in warming of 4.9°C in the NH and 3.8°C in the SH. In addition, the increase in CO_2 warms the tropics by 2.6°C from 1x to 2x PI CO_2 and 3.3°C from 2x to 4x PI CO_2.

Warming patterns with increases in CO_2 are spatially disparate in the high-latitudes. There is more warming over the Arctic from 1x to 2x PI CO_2 and over Antarctica from 2x to 4x PI CO_2 (Fig. 2). Notably, increase of CO_2 in both cases results into more warming over land than over the oceans. Furthermore, seasonal changes show larger warming during boreal winter (DJF) compared to summer (JJA) for both cases of CO_2 increase.

The warming from MCO1x to MCO2x can be generally attributed to clear sky longwave and surface albedo changes (Fig. 3). Over the high-latitudes, the cloudy sky emissivity also

https://doi.org/10.5194/egusphere-2026-899
Preprint. Discussion started: 24 February 2026

contributes surface warming. However, the high-latitude warming is partially offset by heat divergence and increased cloud albedo. The high latitude cloud albedo effects are a result of increased cloud cover in the simulated Miocene climate with increasing CO_2 (Fig. SP2). On the other hand, a reduction in cloud albedo amplifies warming in the midlatitudes and some parts of the tropics (Fig SP2).

Between the MCO4x and MCO2x simulations, surface warming is also largely attributed to reduction in clear sky emissivity. In addition, reduced surface reflection is evident in the high-latitudes, though smaller compared to the changes between the MCO1x and MCO2x simulations. The reduced albedo feedback can be attributed to less sea ice and snow in an already warm climate of MCO2x. Furthermore, there is less reduction in heat convergence between the MCO4x and MCO2x experiments.

For both cases, warming over the tropics and midlatitudes is also partially attributed to reduction in cloud albedo, resulting from decreased cloud cover and less reflection of incoming solar radiation. Overall, our results show longwave emissivity, reduced surface albedo, and reduced cloud albedo are the main drivers of surface warming between the three MCO simulations. This agrees with past Miocene studies (Burls et al., 2021; Sun et al., 2024) and studies about future climate change (e.g., Pithan and Mauritsen, 2014; IPCC 2021).

3.1.2 Precipitation

In the MCO1x experiment, precipitation averages 3.1 mm/day and 1.8 mm/day over the NH and SH high-latitudes, respectively (Fig.1). In the midlatitudes, precipitation is 2.7 mm/day over the NH and 3.1 mm/day over the SH. In the tropics, the mean position of the Intertropical Convergence Zone (ITCZ) is in the SH with maximum annual mean precipitation exceeding 6 mm/day. At 1x PI CO_2, the MCO climate is relatively wet over the mid-latitudes, with more precipitation being received during winter (Fig. 4).

Doubling of CO_2 to 2x PI level results in increased precipitation over the entire zonally averaged NH with larger increases (above 0.6 mm/day) over the high-latitudes and the tropics (Fig. 1). Over the SH, precipitation is enhanced by ~0.3 mm/day over the midlatitudes and by 0.6 mm/day over Antarctica. However, a reduction in precipitation is observed over the SH subtropics and around 65°S.

Regionally, CO_2 induced changes in precipitation from 1x to 2x PI level show increases over most parts of the globe but a reduction over regions of the subtropics, Mediterranean, Central America, Southern Indian Ocean, Southern Ocean, North and Southern Atlantic (Fig. 4). In addition, the Arctic and NH mid and high-latitudes exhibit larger precipitation changes, especially in boreal winter.

Going from MCO2x to MCO4x, precipitation increases more in the SH than the NH. NH mid- and high-latitudes show a precipitation increase of ~0.15 mm/day and a reduction over the Arctic of ~0.1 mm/day. Furthermore, a decrease in precipitation is observed in the subtropics of both hemispheres. Over the SH, increase in CO_2 from 2x to 4x PI results in increased precipitation with greatest increases around 60°S and over Antarctica.

Regionally, increasing CO_2 from 2x to 4x PI levels results in drying over the Arctic and the sub-tropical regions. In addition, seasonal precipitation shows enhanced precipitation over land during DJF and enhanced drying over land during JJA in both hemispheres. Over the ocean, there is an increase in precipitation and a reduction over eastern Pacific and the Atlantic for both seasons with an increase from 2x to 4x PI CO_2.

https://doi.org/10.5194/egusphere-2026-899
Preprint. Discussion started: 24 February 2026

3.1.3 $\delta^{18}O_p$

The MCO1x experiment shows a global mean $\delta^{18}O_p$ of -7.56 ‰ with more depleted values in the high-latitudes of -17 ‰ in the NH and -18 ‰ in the SH (Fig 1). Spatially, the MCO1x experiment reveals relatively enriched values of $\delta^{18}O_p$ over the tropical Atlantic, eastern tropical Pacific, Indian Ocean, and North Africa relative to PI (Fig. 5). Increasing CO_2 to 2x PI level results in enrichment in the values of $\delta^{18}O_p$ with greatest increases over the NH high-latitudes of 2.0 ‰ (Fig. 1). The SH high-latitudes are also enriched by 1.2 ‰. The increase in $\delta^{18}O_p$ from MCO2x to MCO4x is smaller than that from MCO1x to MCO2x, especially over the high-latitudes. In contrast, the midlatitudes reveal greater enrichment in $\delta^{18}O_p$ with increasing CO_2. Interestingly, the tropics show more enrichment in $\delta^{18}O_p$ despite enhanced precipitation over the regions with increasing CO_2.

Regionally, $\delta^{18}O_p$ becomes more enriched over the Arctic, North America and Eurasia with increasing CO_2. In addition, more enriched values are observed over the Arctic during DJF in the MCO2x relative to MCO1x, which is similar to the temperature response. Interestingly, there are more depleted $\delta^{18}O_p$ values over some parts of Antarctica during DJF for MCO2x relative to MCO1x and MCO4x.

Table 1. Global mean surface temperature and meridional temperature gradients between the tropics and high latitudes.

	PI	**MCO1x**	**MCO2x**	**MCO4x**
Surface temperature	14.35	18.44	22.27	26.36
Tropical	26.74	28.67	31.31	34.62
NH high-latitudes	-18.42	-8.82	2.06	8.89
SH high-latitudes	-31.86	-13.03	-6.45	0.04
NH meridional temp gradient	45.16	37.49	29.25	25.73
SH meridional temp gradient	58.60	41.71	37.76	34.59

https://doi.org/10.5194/egusphere-2026-899
Preprint. Discussion started: 24 February 2026

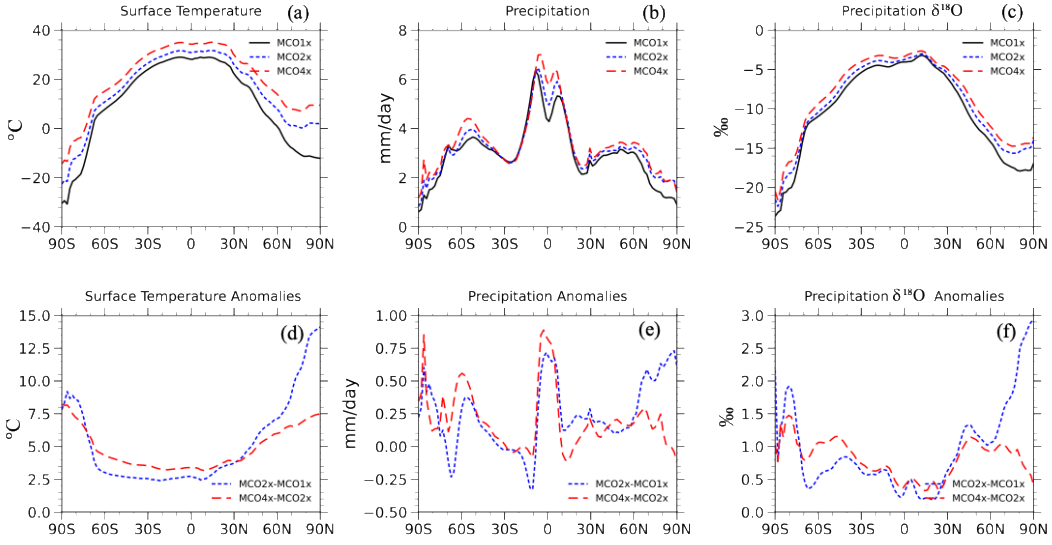

Figure 1. Zonal distribution of mean annual surface temperature, precipitation, and precipitation $\delta^{18}O$ of simulated MCO under 1x, 2x, and 4x PI CO_2. The lower panels show changes with increase in CO_2.

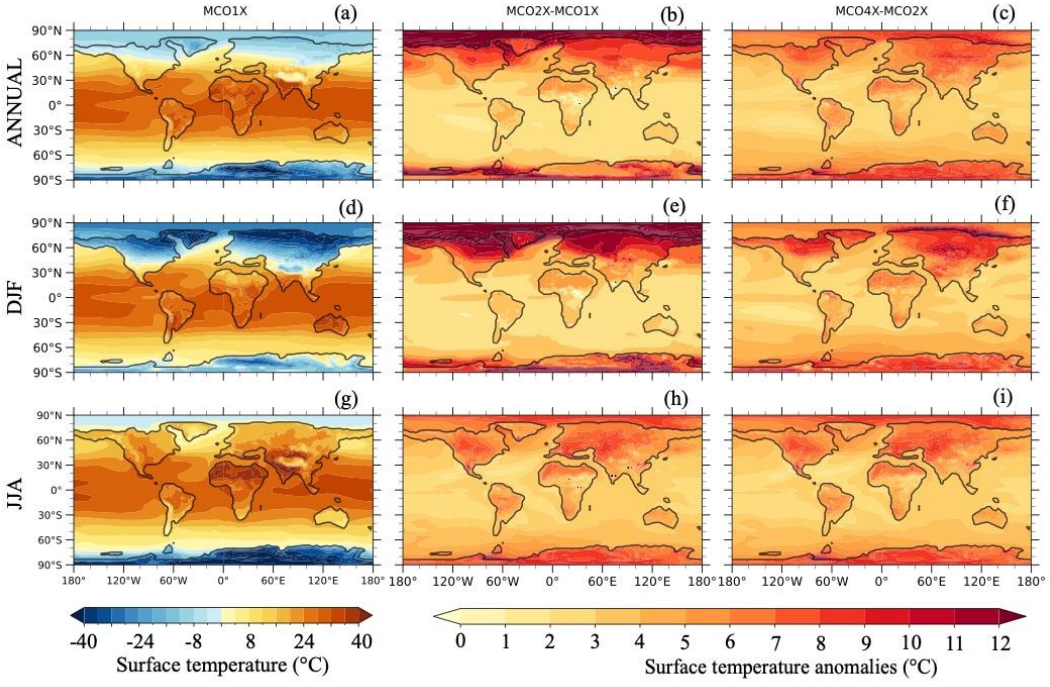

https://doi.org/10.5194/egusphere-2026-899
Preprint. Discussion started: 24 February 2026

Figure 2. Annual (a, b, c) and seasonal mean (DJF; d, e, f and JJA; g, h, i) mean surface temperature of MCO simulations (1x, 2x, and 4x PI CO_2). The stipples show areas where changes are not significant at 95% confidence level.

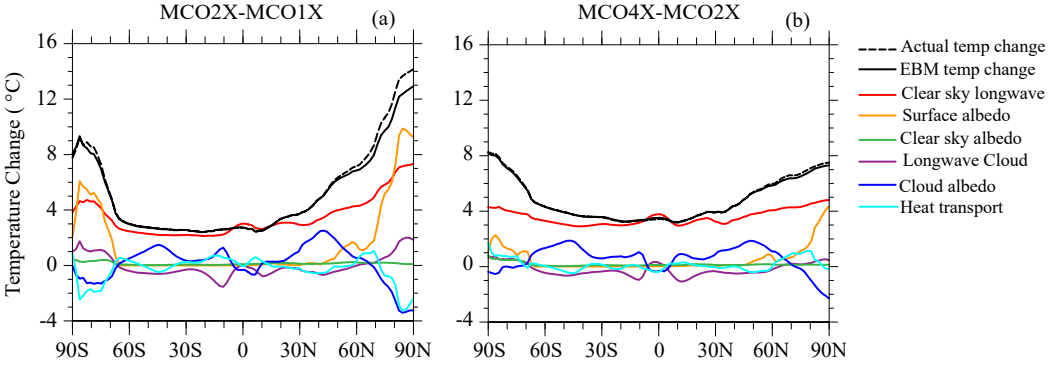

Figure 3. Energy balance analysis of zonal mean annual surface temperature differences between the MCO1x and MCO2x (left) and MCO4x and MCO2x (right) experiments.

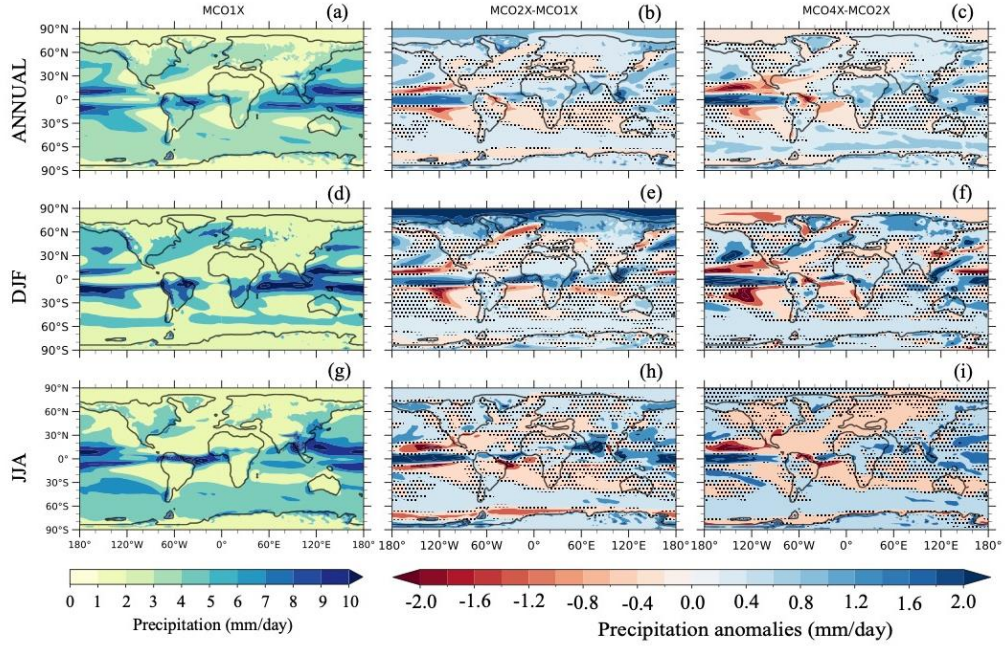

Figure 4. Same as Figure 2 but for precipitation

https://doi.org/10.5194/egusphere-2026-899
Preprint. Discussion started: 24 February 2026

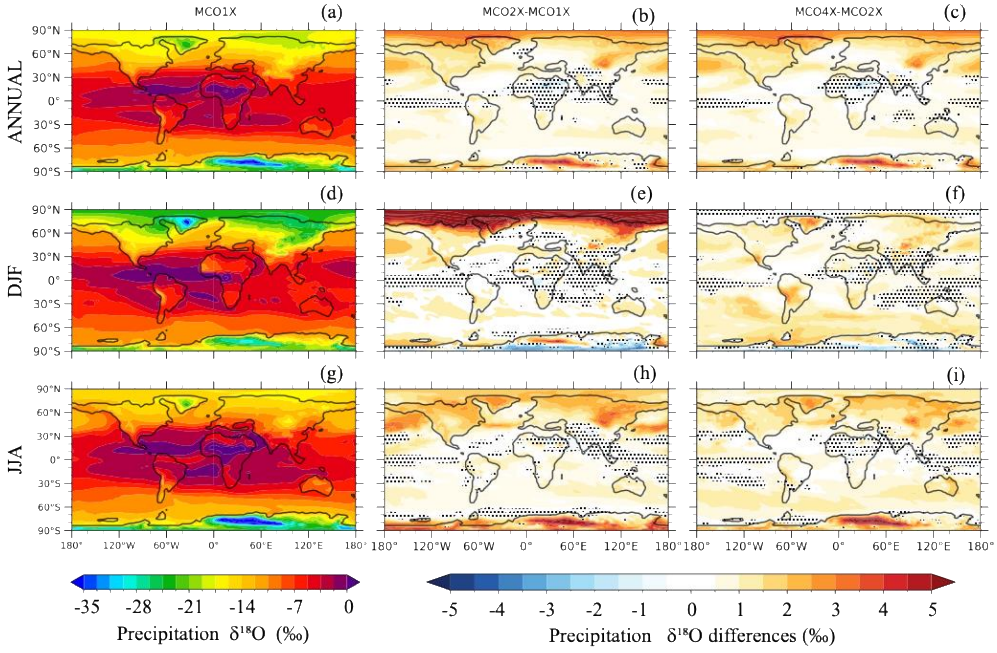

Figure 5. Same as Figure 2 but for precipitation $\delta^{18}O$

3.2 Meridional heat transport

In the MCO1x experiment, atmospheric heat transport peaks at ~42°N/S with 4.4 petawatts (PW) in both the NH and SH (Fig. SP4). Ocean heat transport reaches a maximum of 1.5 PW over the NH and 1.2 PW over the SH. Ocean heat transport peaks at 10°N in the NH and 15°S in the SH. Between MCO1x and MCO2x, the increase in CO_2 results in reduced atmospheric northward heat transport in the NH over the tropics and midlatitudes with the highest decrease between latitudes 30 – 45°N of ~0.31 PW (Fig. 6). In contrast, the SH shows an increase in southward atmospheric heat transport, except south of 65°S, where a small reduction is observed. Comparing MCO4x to MCO2x, there is an increase in northward meridional atmospheric heat transport, especially over the NH tropics and subtropics, with changes up to 0.15 PW. The midlatitudes show a smaller increase in poleward atmospheric heat transport in the NH and a decrease in the SH of less than 0.1 PW. Moreover, increasing CO_2 from 1x to 2x PI results in enhanced poleward ocean heat transport in the NH and a decrease in the SH. The tropics show small changes of less than 0.1 PW whereas large changes are observed over the subtropics and midlatitude with peaks of 0.25 PW. Relative to MCO2x, the MCO4x experiment reveals a large decrease in poleward ocean heat transport over the NH subtropics.

Considering the total required heat transport at the top of the atmosphere (Fig. 6c), there is generally less energy transported polewards in both the NH and SH in the MCO2x compared to MCO1x. This is characterized by an increase in poleward ocean heat transport and a reduction in atmospheric heat transport. In the MCO4x relative to MCO2x, there is a slight increase in total heat transport with a reduction in ocean heat transport being offset by the increase in atmospheric heat transport.

Regional ocean heat transport is greatest in the Pacific with a large amount of northward heat transport in the NH and deepwater formation in the North Pacific (Fig SP7). In contrast,

https://doi.org/10.5194/egusphere-2026-899
Preprint. Discussion started: 24 February 2026

meridional heat transport in the Atlantic is weak and primarily in the SH. Although there are changes in the magnitudes of meridional heat transport between the ocean basins, the general patterns remain the same with increasing CO_2.

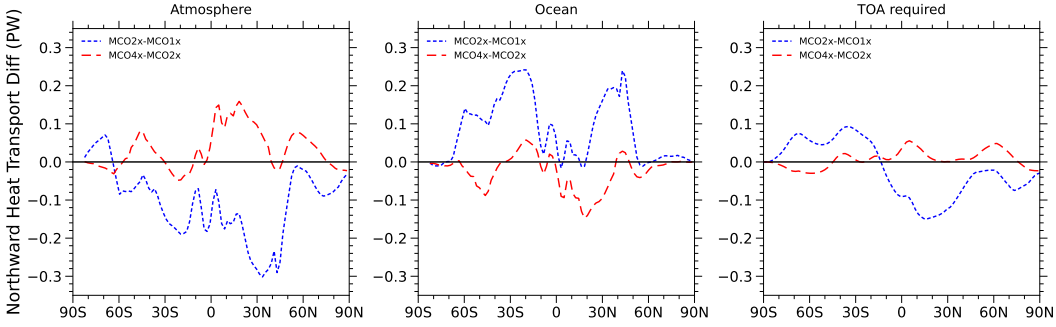

Figure 6. Zonally averaged northward heat transport anomalies for atmosphere (a), ocean (b), and total heat transport (c) between the different MCO experiments.

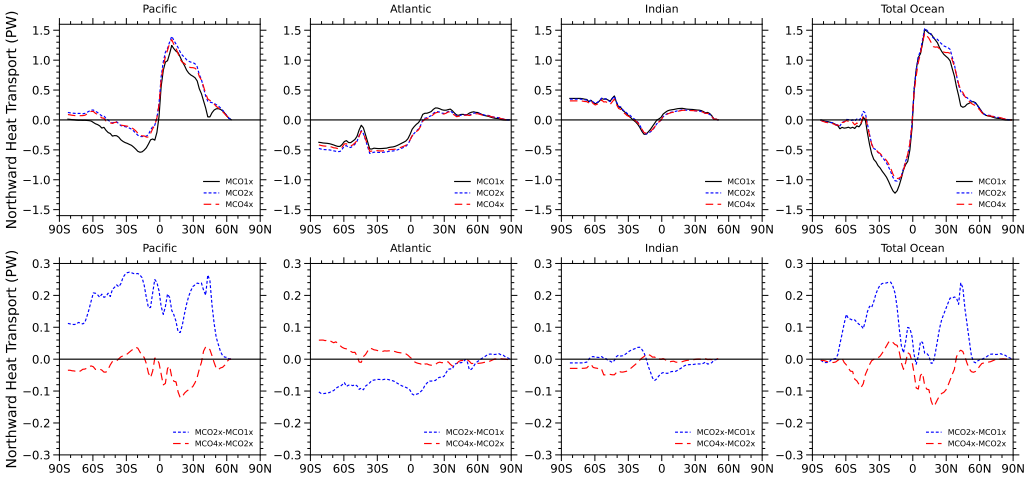

Figure 7. Meridional ocean heat transport by the Pacific, Atlantic and total ocean for the three MCO experiments (top) and the differences between the MCO1x and MCO2x and MCO4x and MCO2x (bottom)

3.3 Comparison with proxy data

We compare model results with reconstructed surface temperature, precipitation, and $\delta^{18}O_p$ to assess which prescribed CO_2 produces better model-proxy agreement (Fig. 8, 9; Table 2). Our simulations reveal a warm bias over the tropics and a cold bias over the high latitudes, especially in the North Atlantic and Arctic. MCO1x shows better agreement with land surface temperature (LST) whereas MCO4x reveals better agreement with SSTs. Some studies have reported a bias in proxy reconstructions stemming from temporal shifts of growing seasons for planktonic organisms (e.g., Lohman et al., 2013). Therefore, we further compared our simulations against seasonal (e.g.,

https://doi.org/10.5194/egusphere-2026-899
Preprint. Discussion started: 24 February 2026

JJA over the NH and DJF over the SH) surface temperatures and found better model-data agreement with MCO2x for SSTs during summer (Fig. SP8).

Model-proxy precipitation comparisons show a model dry bias over most regions in MCO1x (Fig. 8). The largest bias is observed over mountainous and desert regions. Better model-data agreement is observed over East Asia and southern South America. Precipitation reconstructions show best agreement with the MCO2x experiment but with a relatively large RMSE (Table 2). With regards to $\delta^{18}O_p$, there is limited data available during the Miocene and our compilation is limited to the NH (Kukla et al., 2022). Comparison with the available $\delta^{18}O_p$ data shows the best model-data agreement with the MCO1x experiment; however, the differences in RMSE are relatively small between experiments (Fig. 8 and Table 2). Similar to precipitation, the largest biases are observed over high elevation regions such as the Tibetan Plateau and Rocky Mountains.

Table 2. RMSE for comparison of MCO simulations against proxy reconstructions for annual, summer (JJA in NH and DJF in SH), and winter (DJF in NH and JJA in SH). Annual precipitation is calculated in mm/year and seasonal precipitation in mm/day.

		Variable			
		SST	**LST**	**Precip**	**$\delta^{18}O_p$**
Annual	**MCO1x**	8.59	**8.10**	981.4	**6.82**
	MCO2x	5.83	8.76	**926.2**	6.92
	MCO4x	**5.21**	11.67	933.2	6.92
Summer	**MCO1x**	6.70	**10.12**	3.30	7.48
	MCO2x	**4.99**	13.60	**3.00**	7.33
	MCO4x	7.72	18.25	3.29	**7.20**
Winter	**MCO1x**	11.24	12.78	**3.21**	**7.33**
	MCO2x	7.98	9.68	3.23	7.38
	MCO4x	**6.50**	**9.08**	3.35	7.35

https://doi.org/10.5194/egusphere-2026-899
Preprint. Discussion started: 24 February 2026

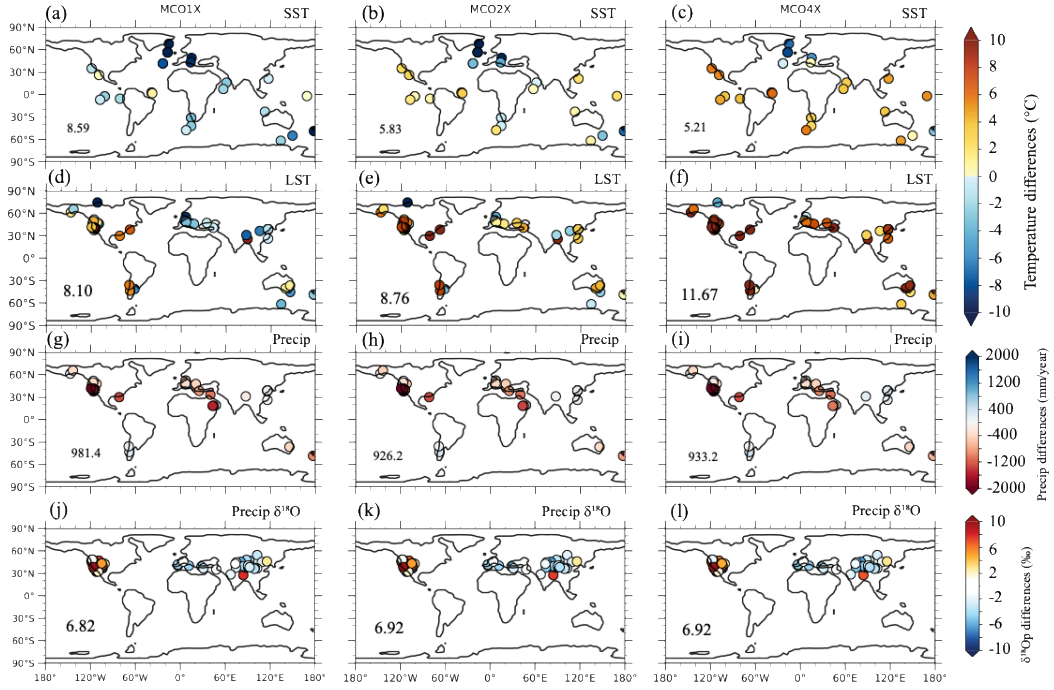

Figure 8. Mean annual sea surface temperature (a, b, c), land surface temperature (d, e, f), precipitation (g, h, i) and precipitation $\delta^{18}O$ (j, k, l) bias of simulated MCO against proxy reconstruction under the different CO_2 forcings.

https://doi.org/10.5194/egusphere-2026-899
Preprint. Discussion started: 24 February 2026

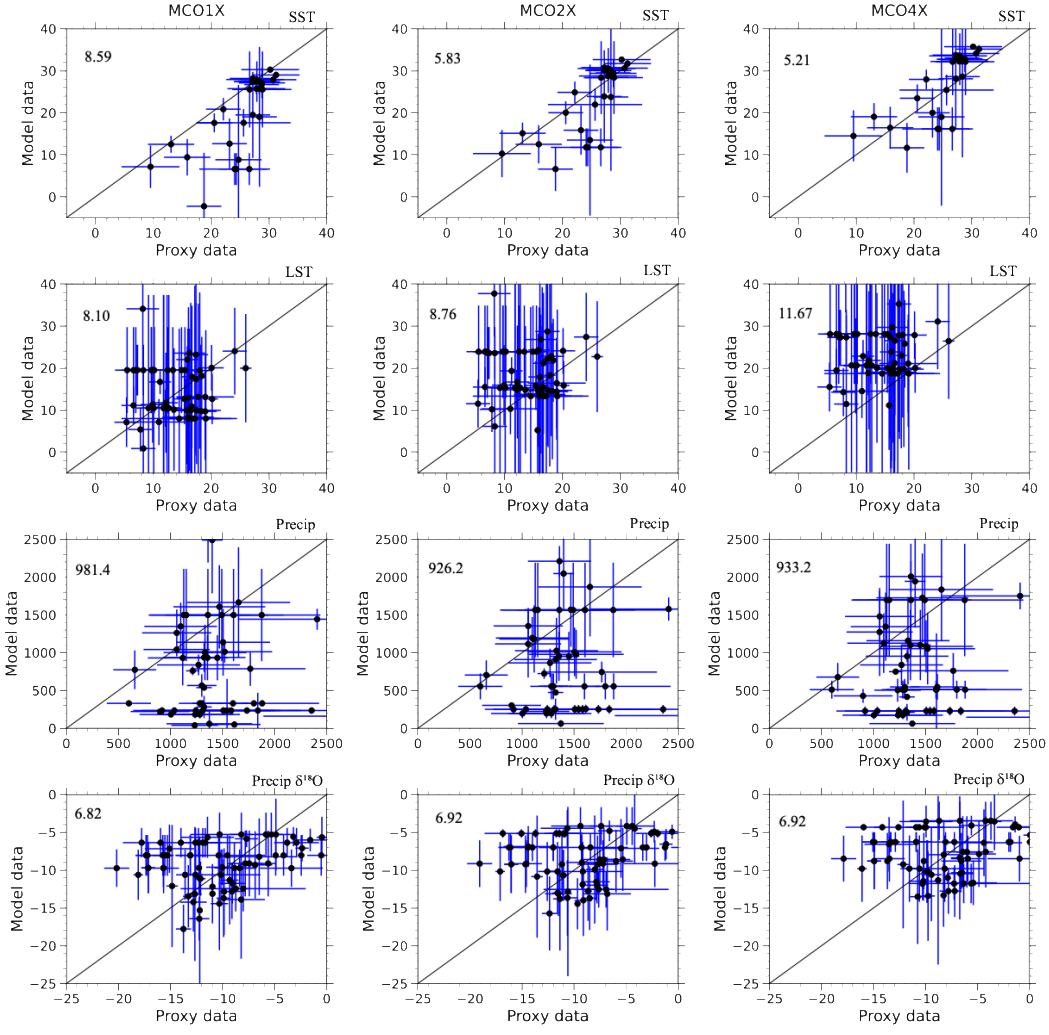

Figure 9 Comparison of model data and proxy data for sea surface temperature (a, b, c), land surface temperature (d, e, f), annual precipitation (g, h, i), and precipitation $\delta^{18}O$ (j, k, l) during the MCO. The error bars show uncertainty for the proxies and the winter to summer seasonal range for the model simulations. The root mean square error over all the sites is shown on the upper left.

3.4 Comparison with preindustrial and future projected climate

3.4.1 Comparison with preindustrial climate

The MCO1x experiment is warmer than the PI experiment with global mean annual temperatures of 18.4°C versus 14.3°C. Therefore, the MCO boundary conditions result into a global warming of 4.1°C. In the NH high-latitudes, MAT is -8.8°C for MCO1x and -18.4°C for PI whereas in the SH high-latitude, MAT is -13.0°C for MCO1x and -31.9°C for PI (Fig. 10a-10b, Fig.10e). The mid-latitude MAT is 11.4°C for MCO1x and 8.9°C for PI in the NH. In the SH, the mid-latitude MAT is 15.6°C and 11.1°C for the MCO1x and PI, respectively. The subtropical MAT is 26.0°C

https://doi.org/10.5194/egusphere-2026-899
Preprint. Discussion started: 24 February 2026

for the MCO1x both in the NH and SH whereas for PI, MAT is 24.2°C in the NH and 23.4°C in the SH. Moreover, MAT in the tropics is also elevated at 28.7°C for the MCO1x relative to 26.7°C for PI. Furthermore, seasonal patterns show pronounced warming over the high-latitudes during winter and over land during summer for MCO1x relative to PI (Fig. SP10).

MCO1x is drier with global mean precipitation of 3.2 mm/day compared to PI with a global mean precipitation of 3.4 mm/day (Fig. 10c-10d). Zonal averages though suggest enhanced precipitation during the MCO relative to PI except at ~60°S (Fig. 10f). Over the high-latitudes, average precipitation is 1.7 mm/day for MCO1x and 1.4 mm/day for PI in the NH, whereas in the SH, average precipitation is 2.1 mm/day for MCO1x and 1.6 mm/day for PI. In the NH mid-latitudes, average precipitation is 2.9 mm/day for MCO1x and 2.7 mm/day for PI. On the other hand, SH mid-latitude precipitation averages at 3.3 mm/day for MCO1x and 3.1 mm/day for PI. Moreover, tropical rainfall maximizes at 6.4 mm/day in the SH during the MCO and 6.5 mm/day in the NH for PI. Generally, larger precipitation differences are observed over the NH midlatitudes, SH high-latitudes, and the tropics. The spatial distribution of precipitation during the MCO relative to PI shows enhanced precipitation over South America and decreased precipitation over eastern and southern Africa. Furthermore, enhanced precipitation is observed over coastal North America, Europe, Eurasia, coastal East Asia, and over the tropics. Over the ocean, enhanced precipitation occurs in the Pacific and Indian oceans. In contrast, a drier pattern is observed over the central Atlantic and west equatorial Pacific and a big part of the North Atlantic. In addition, there is expansion of the tropical rain belt in the MCO1x compared to PI, particularly over the equatorial Pacific and Indian Oceans.

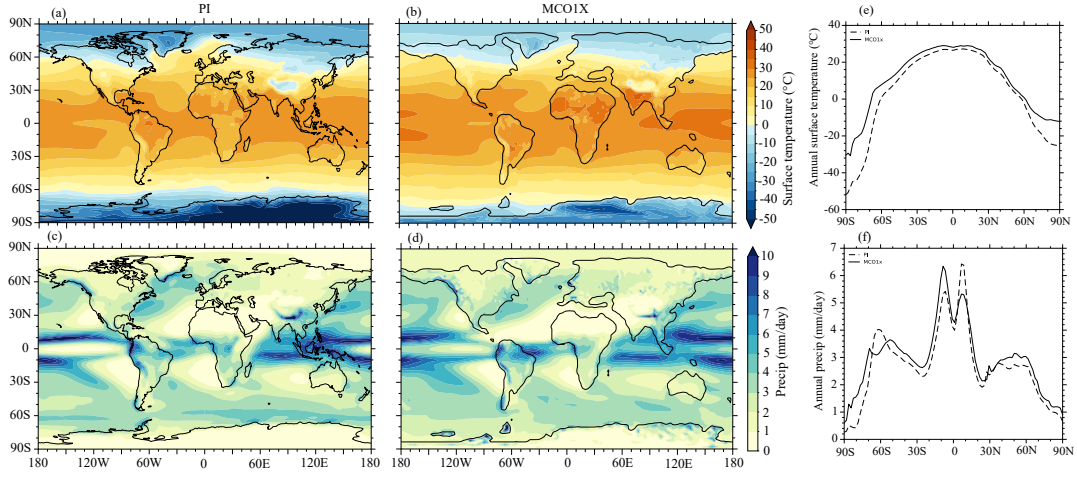

Figure 10. Comparison of simulated MCO climate under 1x PI CO_2 and PI climate for annual mean surface temperature (a, b) precipitation (c, d). The right panel shows the zonal mean annual surface temperature (e), precipitation (f)

3.4.2 Comparison with projected future climate

To compare with future climate projections, we considered climate responses between the MCO1x and MCO2x and projected changes under RCP8.5 relative to PI. Our results show a projected global warming of 4.0°C under RCP8.5 relative to PI and 3.9°C in MCO2x relative to MCO1x. High-latitude temperatures reveal more future warming over the NH and the Southern Ocean but less warming over Antarctica than MCO2x (Fig. 11). In contrast, the midlatitudes show warmer

https://doi.org/10.5194/egusphere-2026-899
Preprint. Discussion started: 24 February 2026

temperatures during the MCO relative to future projections. However, these differences are small. In the tropics and subtropics, both scenarios show similar warming patterns, with average increases of 2.5°C.

Regionally, large warming is observed over the Arctic, followed by Antarctica and the Southern Ocean for both cases. Less spread patterns are observed over the tropics for both the MCO and future projected climate except for North Africa, central South America, and over southwestern Asia. Overall, there are significant differences between LST and SST, with larger warming observed over land than over the ocean and more pronounced changes in the future projections than the MCO (Fig. 11). These differences in warming are especially evident in the JJA seasonal response (Fig. SP13).

Comparing future projected changes in precipitation under RCP 8.5 with PI shows enhanced precipitation of 0.5 mm/day over the mid- and high-latitudes in the NH (Fig.11). Similarly, the MCO2x relative to MCO1x reveals an increase in precipitation over the entire NH, with greatest increases over the high latitudes. However, future projections show a decrease in precipitation over the subtropics and a large increase in precipitation over the tropics of 1.5 mm/day. In the SH, similar responses are observed under RCP8.5: wetter tropics, albeit with a smaller magnitude compared to the NH, drier subtropics, and greatly enhanced precipitation of 0.9 mm/day around 70°S. Similarly, for the Miocene climate, there is enhanced tropical precipitation, drier subtropics, wetter mid- and high-latitudes except around 70°S, where a reduction in precipitation is observed over the SH.

The spatial distribution of precipitation for both the MCO and future projection (Fig. 11) shows more precipitation over the polar regions, the midlatitudes, equatorial regions, and most land areas. In contrast, drier patterns are observed over the subtropics of Europe and the Mediterranean. Our findings are larger for projected changes under RCP8.5 relative to PI than MCO2x relative to MCO1x.

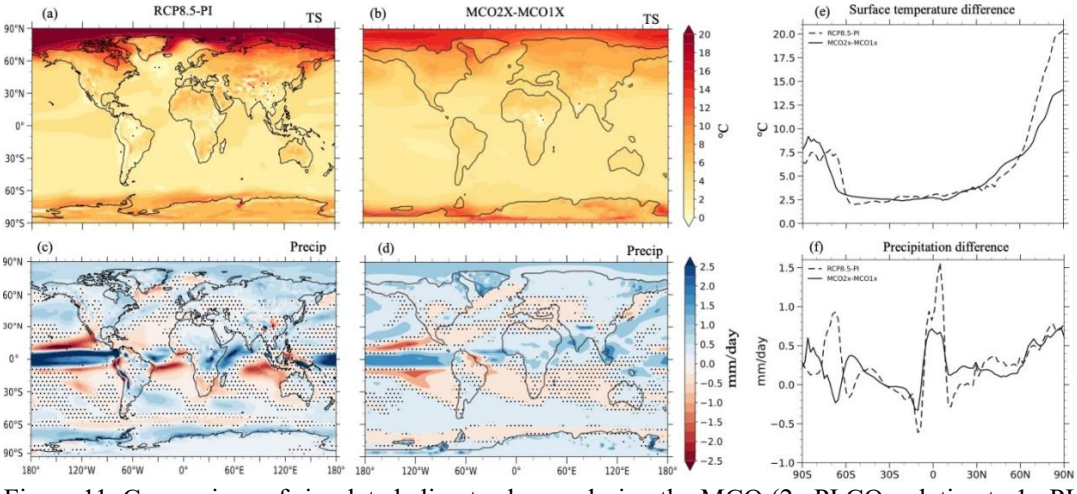

Figure 11. Comparison of simulated climate change during the MCO (2x PI CO_2 relative to 1x PI CO_2) and future projected climate change under RCP8.5 for the period 2080-2100 relative to PI. Shown are maps of changes in annual mean surface temperature (a, b) and precipitation (c, d). The right panels display differences in zonal mean annual surface temperature (e) and precipitation (f).

4 Discussion

https://doi.org/10.5194/egusphere-2026-899
Preprint. Discussion started: 24 February 2026

This study finds that MCO boundary conditions contribute to a global warming of 4.1°C. This contribution of MCO boundary conditions to global warming contrasts with previous studies where non-CO_2 boundary conditions only increased MAT by around 2°C (Krapp and Jungclaus, 2012; Burls et al., 2021). This discrepancy may be a result of differences in paleogeography and the higher climate sensitivity of CESM1 relative to models used for previous Miocene simulations. The CESM1 simulation of the Eocene shows a similarly high sensitivity to boundary conditions with global warming of 5.1°C, which is higher than most models in the DeepMIP ensemble (Lunt et al., 2020).

In our simulations, increasing MCO CO_2 from 1x to 2x PI results in an ECS of 3.9°C, which is lower than the CESM1 ECS of 4.0°C under PI boundary conditions (Gettelman et al., 2019). It is possible that this difference is a result of weakened cryosphere feedbacks associated with a warmer background state during the MCO. However, Earth system models typically show higher ECS with warmer background climate. Indeed, warming from 2x to 4x CO_2, increases the MCO ECS to 4.1°C, which aligns with other studies that find increasing climate sensitivity with warming (Zhu et al., 2021). Our results also highlight the differences in climate responses under equilibrium conditions versus the transient response at year 2100 in the RCP8.5 simulations. Despite significantly less CO_2 forcing, the warming going from MCO1x to MCO2x is comparable to RCP8.5 at year 2100. This result highlights the continued value of efforts to slow CO_2 emissions and enhance CO_2 drawdown as future projections could be underestimating warming due to Earth system feedbacks. Furthermore, the 4.1°C warming from MCO boundary conditions shows that future warming could be significantly higher than predicted if ice sheet and vegetation feedbacks are reconsidered and simulations are run beyond 2100.

The spatial pattern of warming changes significantly with doubling of CO_2 (Fig. 2; 3). High-latitude warming is greater when comparing MCO1x to MCO2x than when comparing MCO2x to MCO4x. Furthermore, polar amplification is more evident over the NH high-latitudes than the SH high-latitudes, especially over the Arctic when increasing CO_2 from 1x to 2x PI. These differences are largely attributed to surface albedo feedbacks linked to changes in sea-ice extent and snow cover; a similar pattern of warming is found in the RCP8.5 simulations. In contrast, tropical and SH mid-latitude warming is larger between MCO2x and MCO4x than between MCO1x and MCO2x due to enhanced water vapor feedbacks in a warmer climate. In particular, low- and mid-latitude land surfaces experience enhanced warming when CO_2 increases from 2x to 4x PI levels.

Our results agree with past studies regarding the different contributions to surface warming for the Miocene (Burls et al., 2021; Sun et al., 2024) and studies about future climate change (Pithan and Mauritsen, 2014; IPCC 2021). In particular, our results agree with previous paleoclimate and future studies which report similar land-sea warming contrasts. Those studies attribute land-sea warming contrasts to differences in land sensible and latent heat fluxes (Sutton et al., 2008), soil moisture reductions (Clark et al., 2010), boundary layer relative humidity and effect of low-level cloud cover changes over land (Fassulo, 2010), and land-ocean boundary layer lapse rate changes (Joshi et al., 2008; Seltezer et al., 2023). This shift in the spatial pattern of warming could have important implications for longer term changes in climate with continued global warming.

The strong reduction in the meridional temperature gradient going from MCO1x to MCO2x can be attributed to cryosphere feedbacks and is associated with a significant reduction in poleward heat transport (Newsom et al., 2021). Interestingly, while the reduction in meridional heat transport from MCO1x to MCO2x is similar in both hemispheres, the mechanisms are distinct

https://doi.org/10.5194/egusphere-2026-899
Preprint. Discussion started: 24 February 2026

(Figure 6; 7). Poleward heat transport in the SH decreases in the ocean but increases in the atmosphere while poleward heat transport in the NH increases in the ocean but decreases in the atmosphere. This partial compensation in meridional heat transport between ocean and atmosphere has been found in many simulations on a variety of timescales (e.g., Farneti and Vallis, 2013). Going from MCO2x to MCO4x, the changes in poleward heat transport are smaller, with almost completely compensating changes in the ocean and atmosphere. However, now NH atmosphere heat transport increases while NH ocean heat transport decreases. This relatively small change in poleward heat transport between MCO2x and MCO4x might be associated with the smaller reduction in latitudinal temperature gradients, and the small increase in atmospheric heat transport possibly attributable to an increase in atmospheric moisture transport in a warmer climate state (Hwang and Frierson, 2010). With both increases in CO_2, the changes in ocean heat transport are largely due to the Pacific associated with a robust Pacific Meridional Overturning Circulation, similar to some other simulations of the Neogene (e.g., Burls et al., 2017).

Comparison with proxy reconstructions shows the best model-data agreement with the MCO1x experiment for terrestrial temperatures and the MCO4x experiment for marine surface temperatures (Fig. 8, 9; Table 2). Moreover, seasonal comparisons show better agreement between the MCO2x experiment and marine records during summer than in the annual mean, suggesting that model-data discrepancies may be reduced when accounting for different growing seasons of planktonic organisms (Lohman et al., 2013). Model-proxy comparison during the MCO remains challenging as proxy records are sparse. However, the large differences between terrestrial and marine surface temperature reconstructions suggests systematic bias in either the proxies or the model simulations. Paleobotanical terrestrial proxies based on modern climatic analogues might suffer a cold bias due to selective extinction of thermophilic species within plant groups, while diversification occurs of cold-adapted species. However, the modern climate analogue based reconstructions are largely congruent with leaf physiognomy-based proxies. Additionally, many mid-latitude MCO paleofloral assemblages have a distinct lack of thermophilic (e.g., tropical) plant groups, which provides strong evidence that these temperate taxa truly reflect temperate climates (Reichgelt et al., 2023). Another potential problem with paleobotanical proxies is the inclusion of wind-dispersed pollen from regional uplands that may mute a local, typically warmer, climatic signal (Mander and Punyasena, 2018). It thus may be preferable to remove pollen assemblages from proxy-model comparisons, despite this leading to a much smaller dataset for comparison (Reichgelt and West, 2025).

Despite the relatively high climate sensitivity of CESM1, the model does not reproduce the meridional temperature gradient suggested by proxy reconstructions of the MCO (Table 1). MCO1x and MCO2x SSTs are relatively congruent with proxy reconstructions in the tropics but the model SST results are colder at high-latitudes. Increasing the CO_2 to 4x PI level improves agreement with SST reconstructions at high-latitudes but the simulated low-latitude sea surface temperatures then becomes too warm. This is similar to the results of previous Miocene climate modeling studies (e.g., Krapp and Jungclaus, 2011; Burls et al., 2021; Sun et al., 2024).

We observe generally wetter conditions in the MCO1x experiment relative to PI. This increase in precipitation with MCO boundary conditions could be the result of changes in circulation from vegetation and ice sheet responses (Feng et al., 2017). Regionally, however, the MCO1x experiment has a drier central America and North Atlantic, which could be due to the open central American seaway, allowing for mixing of Atlantic and Pacific Ocean waters, and therefore, slowing AMOC (Maier-Reimer et al., 1990; Lunt et al., 2007). The MCO simulations also show a southward shift of the ITCZ relative to PI. The shift of maximum tropical precipitation

https://doi.org/10.5194/egusphere-2026-899
Preprint. Discussion started: 24 February 2026

has been attributed to change in the interhemispheric energy budget (Donohoe et al., 2013) resulting from MCO boundary conditions such as reduced Antarctica ice sheets and open tropical ocean gateways (Steinthorsdottir et al., 2021). Similar to future projections, an increase in precipitation is observed over the mid- and high-latitudes with warming, especially when CO_2 levels rise from 1x to 2x PI. This enhanced precipitation has been attributed to a poleward shift of storm tracks (IPCC, 2013). Interestingly, increased CO_2 from 2x to 4x PI level results in enhanced precipitation over land and drier conditions over the Arctic as well as expansion of the dry subtropics over the ocean. Over the ocean, MCO warming shows the "wet getting wetter, and dry getting drier" paradigm (Held and Soden, 2006), similar to hydrologic responses with future warming. On land, precipitation changes generally agree with future warming scenarios and likely reflect complex interactions between circulation changes and thermodynamics (Seager et al., 2010).

Our MCO experiments generally have a dry bias over land relative to precipitation reconstructions. Similar challenges were reported by Acosta et al. (2024) and Herold et al. (2010) where large dry biases were reported, especially in the mid- and high-latitudes. Furthermore, Herold et al. (2010) demonstrated that there is better model-proxy agreement when model SSTs are prescribed with proxy informed values. Therefore, the inability of our model to fully simulate the reduced meridional temperature gradient could also limit its ability to capture the precipitation pattern of the MCO. The discrepancies could also be due to a combination of uncertainty in topography and geography as well as seasonal biases in the proxy reconstructions. Moreover, paleobotanical proxies also tend to have a wet bias as plant fossils are preserved in wetter environments (Reichgelt et al., 2022). Some of the model-proxy disagreements might also be attributed to the relatively low resolution of the model configuration, which prevents it from resolving small scale weather phenomena and topographic effects. In addition, the simulated dry bias could result in warmer surface temperatures as low precipitation leads to low soil moisture, which decreases latent heat flux and increases sensible heat flux (Lin et al., 2017).

$\delta^{18}O_p$ shows enriched values during the MCO relative to PI. $\delta^{18}O_p$ variations tend to follow the variation in surface temperature, especially over the high-latitudes (Dansgaard, 1964). Despite the increase in precipitation with CO_2 over most parts of the globe, there is higher $\delta^{18}O_p$ values in most regions. The enrichment of $\delta^{18}O_p$ with precipitation may be explained by increase in atmospheric moisture residence time in a warm climate, where the abundance of moisture in the atmosphere exceeds local evaporation and precipitation (Singh et al., 2016; Winnick et al., 2014; 2015; Kukla et al., 2019). Our findings also highlight the difficulty ascribing changes in tropical $\delta^{18}O$ to precipitation amount when greenhouse gas concentrations are varying as our simulations do not display amount effect response to CO_2 forcing during the MCO.

5 Conclusion

We present findings of model simulations of the MCO under three different CO_2 forcings of 1x, 2x, and 4x PI level using a water isotope tracer enabled Earth System model (iCESM1.2). Generally, the MCO simulations exhibits warm temperatures relative to preindustrial with largest changes over the high-latitudes attributed to the greenhouse effect and reduced surface albedo. Even with preindustrial CO_2, MCO boundary conditions lead to significant surface warming relative to present-day. The MCO in our simulations also has enhanced precipitation in the mid and high-latitudes, and the ITCZ shifts southward. Overall, better model-data agreement exists with the 1x PI CO_2 for terrestrial records and 4x PI CO_2 for marine records. However, all our simulations still underestimate the reduced meridional temperature gradient reconstructed by

https://doi.org/10.5194/egusphere-2026-899
Preprint. Discussion started: 24 February 2026

proxy records. In addition, the simulated MCO climate under 2x PI CO_2 is warmer than future climate projections under RCP8.5, despite lower CO_2, due to differences in boundary conditions and transient versus equilibrium climate response. Although this makes comparisons with future climate challenging, the MCO still provides valuable insights into Earth system responses to warmer than present conditions and a valuable test for Earth system models.

Acknowledgement

The authors are grateful to the National Science Foundation (NSF) for funding this work under grant EAR-2002440 awarded to CRT. Much appreciation is also extended to the Computational Information Systems Laboratory at the National Center for Atmospheric Research (NCAR, Colorado) also supported by the NSF for providing computing resources and model codes. HNN is also thankful to the Intergovernmental Panel on Climate Change (IPCC) and the Prince Albert II of Monaco Foundation for additional funding towards this work through the IPCC Scholarship.

Author contribution

H.N.N and C.R.T conceptualized the work and set up the model runs. H.N.N carried out formal analysis and wrote the first draft. C.R.T supervised and edited the write up. R.F setup the model boundary conditions and provided the script for energy balance model analysis. L.X carried out the meridional heat transport analysis. T.R provided terrestrial proxy data of temperature and precipitation for comparison with the model simulations. D.I provided insights into oxygen isotope data. A.L provided the reconstructed isotope proxy modern locations to paleo locations. All authors edited the manuscript.

Data availability

Miocene Climatic Optimum and preindustrial iCESM model outputs used in the study are available upon request. CESM1 large ensemble for future projections can be accessed at https://www.earthsystemgrid.org/dataset/ucar.cgd.ccsm4.cesmLE.html. Proxy temperature reconstruction data is available from Burls et al. (2021) at https://github.com/nburls/MioMIP1 and additional data is available in the Zenodo repository (https://doi.org/10.5281/zenodo.18651533, Nadoya, 2026). $\delta^{18}O$ data used from Kukla et al. (2022) compilation can be accessed at the Paleo Analysis of Terrestrial Climate and Hydrology (PATCH) Lab database, available at https://geocentroid.shinyapps.io/PATCH-Lab/.

Conflict of interest

All authors declare no conflict of interest.

References

Acosta, R. P., Burls, N. J., Pound, M. J., Bradshaw, C. D., De Boer, A. M., Herold, N., et al.: A model-data comparison of the hydrological response to Miocene warmth: Leveraging the MioMIP1 opportunistic multi-model ensemble. Paleoceanography and Paleoclimatology, 39, e2023PA004726. https://doi.org/10.1029/2023PA004726, 2024

Annan, J. D., Hargreaves, J. C., Mauritsen, T., McClymont, E., and Ho, S. L.: Can we reliably reconstruct the mid-Pliocene Warm Period with sparse data and uncertain models?, Clim. Past, 20, 1989–1999, https://doi.org/10.5194/cp-20-1989-2024, 2024.

https://doi.org/10.5194/egusphere-2026-899
Preprint. Discussion started: 24 February 2026

Boschman, L. M.: Andean Mountain building since the Late Cretaceous: A paleoelevation reconstruction. *Earth-Science Reviews*, *220*, 103640, 2021

Bradshaw, C. D., Fletcher, T., Reichgelt, T., Akgün, F., Cantrill, D. J., Casas-Gallego, M., ... & Burls, N.: MioVeg1: A global Middle Miocene vegetation reconstruction for climate modeling. *Paleoceanography and Paleoclimatology*, *40*(11), e2025PA005213, 2025.

Bradshaw, C. D., Langebroek, P. M., Lear, C. H., Lunt, D. J., Coxall, H. K., Sosdian, S. M., & de Boer, A. M.: Hydrological impact of Middle Miocene Antarctic ice-free areas coupled to deep ocean temperatures. *Nature Geoscience*, *14*(6), 429-436, 2021.

Bradshaw, C. D., Lunt, D. J., Flecker, R., and Davies-Barnard, T.: Disentangling the roles of late Miocene palaeogeography and vegetation: Implications for climate sensitivity. Palaeogeography, Palaeoclimatology, Palaeoecology, 417, 17–34. https://doi.org/10.1016/j.palaeo.2014.10.003, 2015

Brady, E., Stevenson, S., Bailey, D., Liu, Z., Noone, D., Nusbaumer, J., et al.: The connected isotopic water cycle in the Community Earth System Model version 1. Journal of Advances in Modeling Earth Systems, 11, 2547–2566. https://doi.org/10.1029/2019MS001663, 2019

Brassell, S. C.: Climatic influences on the Paleogene evolution of alkenones, Paleoceanography, 29, 255-272, doi:10.1002/2013PA002576, 2014.

Burls, N. J., Bradshaw, C. D., De Boer, A. M., Herold, N., Huber, M.: Simulating Miocene warmth: Insights from an opportunistic multi-model ensemble (MioMIP1). Paleoceanography and Paleoclimatology, 36, e2020PA004054. https://doi.org/10.1029/2020PA004054, 2021

Burls, N. J., Fedorov, A. V., Sigman, D. M., Jaccard, S. L., Tiedemann, R., & Haug, G. H.: Active Pacific meridional overturning circulation (PMOC) during the warm Pliocene. *Science Advances*, *3*(9), e1700156, 2017.

Byrne, M. P., & O'Gorman, P. A.: Link between land-ocean warming contrast and surface relative humidities in simulations with coupled climate models. *Geophysical Research Letters*, *40*(19), 5223-5227, 2013.

Byrne, M. P., Pendergrass, A. G., Rapp, A. D., and Wodzicki, K. R.: Response of the Intertropical Convergence Zone to Climate Change: Location, Width, and Strength, Curr. Clim. Chang. Reports, 4, 355–370, 2018

Byrne, M. P.: Amplified warming of extreme temperatures over tropical land. *Nature* Geoscience, 14(11), 837-841, 2021.

Campbell, J., Poulsen, C. J., Zhu, J., Tierney, J. E., and Keeler, J.: CO_2-driven and orbitally driven oxygen isotope variability in the Early Eocene. *Climate of the Past*, *20*(3), 495-522, 2024

Cenozoic CO2 Proxy Integration Project (CenCO2PIP) Consortium*†, Hönisch, B., Royer, D. L., Breecker, D. O., Polissar, P. J., Bowen, G. J., ... & Zhang, L.: Toward a Cenozoic history of atmospheric CO2. *Science*, *382*(6675), eadi5177, 2023.

Cenozoic CO2 Proxy Integration Project (CenCO2PIP) Consortium*†, Hönisch, B., Royer, D. L., Breecker, D. O., Polissar, P. J., Bowen, G. J., ... & Zhang, L.: Toward a Cenozoic history of atmospheric CO2. *Science*, *382*(6675), eadi5177, 2023.

Cook, B. I., Smerdon, J. E., Seager, R., & Coats, S.: Global warming and 21 st century drying. *Climate dynamics*, *43*, 2607-2627, 2014.

Dansgaard, W.: Stable isotopes in precipitation, Tellus, 16:4, 436-468, doi: 10.3402/tellusa.v16i4.8993, 1964

de Nooijer, W., Zhang, Q., Li, Q., Zhang, Q., Li, X., Zhang, Z., ... and Brierley, C. M.: Evaluation of Arctic warming in mid-Pliocene climate simulations. *Climate of the Past Discussions*, *2020*, 1-30. doi.org/10.5194/gmd-4-571-2011, 2020

https://doi.org/10.5194/egusphere-2026-899
Preprint. Discussion started: 24 February 2026

643 Donohoe, A., Marshall, J., Ferreira, D., Armour, K., & McGee, D.: The interannual variability of
644 tropical precipitation and interhemispheric energy transport. *Journal of Climate*, *27*(9), 3377-
645 3392, 2014
646 Farnsworth, A., Lunt, D. J., O'Brien, C. L., Foster, G. L., Inglis, G. N., Markwick, P., et al.:
647 Climate sensitivity on geological timescales controlled by nonlinear feedbacks and ocean
648 circulation. Geophysical Research Letters, 46, 9880–9889.
649 https://doi.org/10.1029/2019gl083574, 2019
650 Feng, R., Bhattacharya, T., Otto-Bliesner, B. L., Brady, E. C., Haywood, A. M., Tindall, J. C., ...
651 & Peltier, W. R.: Past terrestrial hydroclimate sensitivity controlled by Earth system
652 feedbacks. *Nature Communications*, *13*(1), 1306, 2022.
653 Feng, R., Otto-Bliesner, B. L., Fletcher, T. L., Tabor, C. R., Ballantyne, A. P., & Brady, E. C.:
654 Amplified Late Pliocene terrestrial warmth in northern high latitudes from greater radiative
655 forcing and closed Arctic Ocean gateways. *Earth and Planetary Science Letters*, *466*, 129-
656 138, 2017.
657 Ferreira, D., Cessi, P., Coxall, H. K., De Boer, A., Dijkstra, H. A., Drijfhout, S. S., ... & Wills, R.
658 C.: Atlantic-Pacific asymmetry in deep water formation. *Annual Review of Earth and*
659 *Planetary Sciences*, *46*(1), 327-352, 2018.
660 Frigola, A., Prange, M., Schulz, M.: Boundary conditions for the Middle Miocene Climate
661 Transition (MMCT v1.0. Geosci. Model Dev., 11, 1607–1626. https://doi.org/10.5194/gmd-
662 11-1607-2018, 2018
663 Gasson, E., DeConto, R. M., Pollard, D., & Levy, R. H.: Dynamic Antarctic ice sheet during the
664 early to mid-Miocene. *Proceedings of the National Academy of Sciences*, *113*(13), 3459-3464,
665 2016.
666 Gettelman, A., Hannay, C., Bacmeister, J. T., Neale, R. B., Pendergrass, A. G., Danabasoglu, G.,
667 ... & Mills, M. J.: High climate sensitivity in the Community Earth System Model version 2
668 (CESM2). *Geophysical Research Letters*, *46*(14), 8329-8337, 2019.
669 Gibson, M. E., McCoy, J., O'Keefe, J. M. K., Ota.o, N. B. N., Warny, S., & Pound, M. J.:
670 Reconstructing terrestrial paleoclimates: A comparison of the co-existence approach,
671 Bayesian and probability reconstruction techniques using the UK Neogene.
672 Paleoceanography and Paleoclimatology, 37(2), 1–18.
673 https://doi.org/10.1029/2021PA004358, 2022
674 Giorgi, F., Raffaele, F., and Coppola, E.: The response of precipitation characteristics to global
675 warming from climate projections, Earth Syst. Dynam., 10, 73–89,
676 https://doi.org/10.5194/esd-10-73-2019, 2019
677 Goldner, A., Herold, N., & Huber, M.: The challenge of simulating the warmth of the mid-Miocene
678 climatic optimum in CESM1. Climate of the Past, 10(2), 523–536. https://doi.org/10.5194/cp-
679 10-523-2014, 2014
680 Greenop, R., Foster, G. L., Wilson, P. A., & Lear, C. H.: Middle Miocene climate instability
681 associated with high-amplitude CO2 variability. *Paleoceanography*, *29*(9), 845-853, 2014.
682 Grossman, E. L., & Ku, T. L.: Oxygen and carbon isotope fractionation in biogenic aragonite:
683 temperature effects. *Chemical Geology: Isotope Geoscience Section*, *59*, 59-74, 1986.
684 Haywood, A. M., Dowsett, H. J., Robinson, M. M., Stoll, D. K., Dolan, A. M., Lunt, D. J., ... &
685 Chandler, M. A.: Pliocene Model Intercomparison Project (PlioMIP): experimental design
686 and boundary conditions (experiment 2). *Geoscientific Model Development*, *4*(3), 571-577,
687 2011.

https://doi.org/10.5194/egusphere-2026-899
Preprint. Discussion started: 24 February 2026

Haywood, A. M., Tindall, J. C., Burton, L. E., Chandler, M. A., Dolan, A. M., Dowsett, H. J., ... & Salzmann, U.: Pliocene model Intercomparison Project phase 3 (PlioMIP3)–Science plan and experimental design. *Global and Planetary Change*, *232*, 104316, 2024.

Haywood, A. M., Tindall, J. C., Dowsett, H. J., Dolan, A. M., Foley, K. M., Hunter, S. J., ... & Lunt, D. J.: A return to large-scale features of Pliocene climate: The Pliocene Model Intercomparison Project Phase 2. *Climate of the Past Discussions*, *2020*, 1-40, 2020.

Herbert, T. D., Lawrence, K. T., Tzanova, A., Peterson, L. C., Caballero-Gill, R., & Kelly, C. S.: Late Miocene global cooling and the rise of modern ecosystems. Nature Geoscience, 9(11), 843-847, 2016.

Herold, N., Huber, M., & Müller, R. D.: Modeling the Miocene Climatic optimum. Part I: Land and atmosphere. Journal of Climate, 24, 6353–6372. https://doi.org/10.1175/2011JCLI4035.1, 2011

Herold, N., Seton, M., Müller, R. D., You, Y., & Huber, M.: Middle Miocene tectonic boundary conditions for use in climate models. Geochemistry, Geophysics. Geosystems, 9(10), Q10009. https://doi.org/10.1029/2008gc002046, 2008

Hill, D. J., Haywood, A. M., Lunt, D. J., Hunter, S. J., Bragg, F. J., Contoux, C., ... & Ueda, H.: Evaluating the dominant components of warming in Pliocene climate simulations. *Climate of the Past*, *10*(1), 79-90, 2014.

Holbourn, A. E., Kuhnt, W., Lyle, M., Schneider, L., Romero, O., & Andersen, N.: Middle Miocene climate cooling linked to intensification of eastern equatorial Pacific upwelling. Geology, 42, 19–22. https://doi.org/10.1130/G34890.1, 2014

Holland, K., Branson, O., Haynes, L. L., H.nisch, B., Allen, K. A., Russell, A. D., et al.: Constraining multiple controls on planktic foraminifera Mg/Ca. Geochimica et Cosmochimica Acta, 273, 116–136. https://doi.org/10.1016/j.gca.2020.01.015, 2020

Hollis, C. J., Dunkley Jones, T., Anagnostou, E., Bijl, P. K., Cramwinckel, M. J., Cui, Y., et al.: The DeepMIP contribution to PMIP4: Methodologies for selection, compilation and analysis of latest Paleocene and early Eocene climate proxy data, incorporating version 0.1 of the DeepMIP database. Geoscientific Model Development, 12, 3149–3206. https://doi.org/10.5194/gmd-12-3149-2019, 2019

Hu, J., Emile-Geay, J., Nusbaumer, J., & Noone, D.: Impact of convective activity on precipitation δ18O in isotope-enabled general circulation models. Journal of Geophysical Research: Atmospheres, 123, 13,595–13,610. https://doi.org/10.1029/2018JD029187, 2018

Hunke, E. C.: Thickness sensitivities in the CICE sea ice model. *Ocean Modelling*, *34*(3-4), 137-149, 2010.

Hwang, Y. T., & Frierson, D. M.: Increasing atmospheric poleward energy transport with global warming. *Geophysical Research Letters*, *37*(24), 2010.

Intergovernmental Panel on Climate Change (IPCC): Climate Change 2013. The Physical Science Basis. Contribution of Working Group I to the Fifth Assessment Report of the Intergovernmental Panel on Climate Change, edited by: Stocker, T. F., Dahe, Q., Plattner, G.-K., Tignor, M. M. B., Allen, S. K., Boschung, J., Nauels, A., Xia, Y., Bex, V., and Midgley, P. M., Cambridge University Press, Cambridge, United Kingdom and New York, NY, USA, 1029 pp., 2013.

Jia, G., Wang, X., Guo, W., & Dong, L.: Seasonal distribution of archaeal lipids in surface water and its constraint on their sources and the TEX86 temperature proxy in sediments of the South China Sea. *Journal of Geophysical Research: Biogeosciences*, *122*(3), 592-606, 2017.

https://doi.org/10.5194/egusphere-2026-899
Preprint. Discussion started: 24 February 2026

Kay, J. E., Deser, C., Phillips, A., Mai, A., Hannay, C., Strand, G., ... & Vertenstein, M.: The Community Earth System Model (CESM) large ensemble project: A community resource for studying climate change in the presence of internal climate variability. *Bulletin of the American Meteorological Society*, *96*(8), 1333-1349, 2015.

Kim, S. T., & O'Neil, J. R.: Equilibrium and nonequilibrium oxygen isotope effects in synthetic carbonates. *Geochimica et cosmochimica acta*, *61*(16), 3461-3475, 1997.

Knauth, L. P., & Epstein, S.: Hydrogen and oxygen isotope ratios in nodular and bedded cherts. *Geochimica et Cosmochimica Acta*, *40*(9), 1095-1108, 1976.

Knorr, G., & Lohmann, G.: Climate warming during Antarctic ice sheet expansion at the Middle Miocene transition. Nature Geosciences,7(5), 376–381. https://doi.org/10.1038/ngeo2119, 2014

Kochhann, K. G. D., Holbourn, A. E., Kuhnt, W., & Xu, J.: Eastern equatorial Pacific benthic foraminiferal distribution and deep-water temperature changes during the early to middle Miocene. Marine Micropaleontology, 133, 28–39. https://doi.org/10.1016/j.marmicro.2017.05.002, 2017

Kolodny, Y., Luz, B., & Navon, O.: Oxygen isotope variations in phosphate of biogenic apatites, I. Fish bone apatite—Rechecking the rules of the game,1983

Krapp, M and Jungclaus, J.H.: The Middle Miocene climate as modelled in an atmosphere-ocean-biosphere model. Clim. Past, 7, 1169–1188. www.clim-past.net/7/1169/2011/, 2011

Kukla, T., Rugenstein, J. K., Driscoll, E., Ibarra, D. E., & Chamberlain, C. P.: The PATCH Lab v1. 0: A database and workspace for Cenozoic terrestrial paleoclimate and environment reconstruction. *American Journal of Science*, *322*(10), 1124-1158, 2022.

Kukla, T., Winnick, M. J., Maher, K., Ibarra, D. E., & Chamberlain, C. P.: The sensitivity of terrestrial $\delta^{18}O$ gradients to hydroclimate evolution. Journal of Geophysical Research: Atmospheres, 124(2), 563-582, 2019.

Kürschner, W., Kvaˇcek, Z., and Dilcher, D.: The impact of Miocene atmospheric carbon dioxide fluctuations on climate and the evolution of terrestrial ecosystems, Proceedings of the National Academy of Sciences, 105, 449, doi:10.1073/pnas.0708588105, 2008.

Land, L. S.: The application of stable isotopes to studies of the origin of dolomite and to problems of diagenesis of clastic sediments, 1983.

Lin, Y., Dong, W., Zhang, M., Xie, Y., Xue, W., Huang, J., & Luo, Y.: Causes of model dry and warm bias over central US and impact on climate projections. *Nature Communications*, *8*(1), 881, 2017

Liu, X., Herold, N., & Huber, M.: Atlantic meridional overturning circulation influence on the annual mean intertropical convergence zone location in the Miocene. Geophysical Research Letters, 51,e2024GL109159. https://doi.org/10.1029/2024GL109159, 2024

Lohmann, G., Pfeiffer, M., Laepple, T., Leduc, G., & Kim, J. H.: A model–data comparison of the Holocene global sea surface temperature evolution. *Climate of the Past*, *9*(4), 1807-1839, 2013.

Longinelli, A., & Nuti, S.: Revised phosphate–water isotopic temperature scale. Earth and Planetary Science Letters, 19, 373–376, 1973.

Lopes dos Santos, R. A., Prange, M., Casta.eda, I. S., Schefu., E., Mulitza, S., Schulz, M., et al.: Glacial-interglacial variability in Atlantic meridional overturning circulation and thermocline adjustments in the tropical North Atlantic. Earth and Planetary Science Letters, 300, 407–414. https://doi.org/10.1016/j.epsl.2010.10.030, 2010

https://doi.org/10.5194/egusphere-2026-899
Preprint. Discussion started: 24 February 2026

Lunt, D. J., Elderfield, H., Pancost, R., Ridgwell, A., Foster, G. L., Haywood, A., ... & Valdes, P.: Warm climates of the past—a lesson for the future?. *Philosophical Transactions of the Royal Society A: Mathematical, Physical and Engineering Sciences*, *371*(2001), 20130146, 2013.

Lunt, D. J., Haywood, A. M., Schmidt, G. A., Salzmann, U., Valdes, P. J., Dowsett, H. J., & Loptson, C. A.: On the causes of mid-Pliocene warmth and polar amplification. *Earth and Planetary Science Letters*, *321*, 128-138, 2012.

Lunt, D. J., Huber, M., Anagnostou, E., Baatsen, M. L. J., Caballero, R., DeConto, R., Dijkstra, H. A., Donnadieu, Y., Evans, D., Feng, R., Foster, G. L., Gasson, E., von der Heydt, A. S., Hollis, C. J., Inglis, G. N., Jones, S. M., Kiehl, J., Kirtland Turner, S., Korty, R. L., Kozdon, R., Krishnan, S., Ladant, J.-B., Langebroek, P., Lear, C. H., LeGrande, A. N., Littler, K., Markwick, P., Otto-Bliesner, B., Pearson, P., Poulsen, C. J., Salzmann, U., Shields, C., Snell, K., Stärz, M., Super, J., Tabor, C., Tierney, J. E., Tourte, G. J. L., Tripati, A., Upchurch, G. R., Wade, B. S., Wing, S. L., Winguth, A. M. E., Wright, N. M., Zachos, J. C., and Zeebe, R. E.: The DeepMIP contribution to PMIP4: experimental design for model simulations of the EECO, PETM, and pre-PETM (version 1.0), Geosci. Model Dev., 10, 889–901, https://doi.org/10.5194/gmd-10-889-2017, 2017.

Lunt, D., Valdes, P., Haywood, A., and Rutt, I.: Closure of the Panama Seaway during the Pliocene: implications for climate and Northern Hemisphere glaciation, Clim. Dynam., 30, 1–18, doi:10.1007/s00382-007-0265-6, 2007.

Maier-Reimer, E., Mikolajewicz, U., and Crowley, T.: Ocean General Circulation Model Sensitivity Experiment with an open Central American Isthmus, Paleoceanography, 5, 349–366, doi:10.1029/PA005i003p00349, 1990.

Mander, L., Punyasena, S.W.: Fossil pollen and spores in paleoecology. In: Croft D., Su D., Simpson S. (eds) Methods in Paleoecology. Vertebrate Paleobiology and Paleoanthropology. Springer, Cham. 215–234, 2018.

Masson-Delmotte, V., Zhai, P., Pirani, A., Connors, S. L., Péan, C., Berger, S., ... & Zhou, B.: Climate change 2021: the physical science basis. *Contribution of working group I to the sixth assessment report of the intergovernmental panel on climate change*, *2, 2021*.

McClymont, E. L., Ford, H. L., Ho, S. L., Tindall, J. C., Haywood, A. M., Alonso-Garcia, M., ... & Zhang, Z.: Lessons from a high-CO 2 world: an ocean view from~ 3 million years ago. *Climate of the Past*, *16*(4), 1599-1615, 2020.

Miller, K. G., & Katz, M. E.: Oligocene to Miocene benthic foraminiferal and abyssal circulation changes in the North Atlantic. Micropaleontology, 33, 97–149. www.jstor.org/stable/1485489, 1987

Müller, I. A., Fernandez, A., Radke, J., van Dijk, J., Bowen, D., Schwieters, J., & Bernasconi, S. M.: Carbonate clumped isotope analyses with the long-integration dual-inlet (LIDI) workflow: Scratching at the lower sample weight boundaries. Rapid Communications in Mass Spectrometry, 31(12), 1057–1066. https://doi.org/10.1002/rcm.7878, 2017

Müller, P. J., Kirst, G., Ruhland, G., von Storch, I., & Rosell-Melé, A.: Calibration of the alkenone paleotemperature index U37K′ on core-tops from the eastern South Atlantic and the global ocean (60◦N–60◦S). Geochimica et Cosmochimica Acta, 62, 1757–1772, 1998.

Nadoya, N.H.: Terrestrial Terrestrial surface temperature and mean precipitation during the Miocene Climatic Optimum. Zenodo data repository. https://doi.org/10.5281/zenodo.18651533, 2026

https://doi.org/10.5194/egusphere-2026-899
Preprint. Discussion started: 24 February 2026

Neale, R. B., Chen, C., Gettelman, A., Lauritzen, P. H., Park, S., Williamson, D. L., et al.: Description of the NCAR Community Atmosphere Model (CAM 5.0). NCAR Technical Note Scientific and Technical Report, NCAR/TN-486+STR, 2010.

Newsom, E. R., Thompson, A. F., Adkins, J. F., & Galbraith, E. D.: A hemispheric asymmetry in poleward ocean heat transport across climates: Implications for overturning and polar warming. *Earth and Planetary Science Letters*, *568*, 117033, 2021.

Noone, D., & Simmonds, I.: Annular variations in moisture transport mechanisms and the abundance of δ18O in Antarctic snow. Journal of Geophysical Research, 107(D24), 4742. https://doi.org/10.1029/2002JD002262, 2002

Noone, D.: Pairing measurements of the water vapor isotope ratio with humidity to deduce atmospheric moistening and dehydration in the tropical midtroposphere. Journal of Climate, 25(13), 4476–4494. https://doi.org/10.1175/JCLI-D-11-00582.1, 2012

Noone, D.: The influence of midlatitude and tropical overturning circulation on the isotopic composition of atmospheric water vapor and Antarctic precipitation. Journal of Geophysical Research, 113, D04102. https://doi.org/10.1029/2007JD008892, 2008

Oleson, K. W., Lawrence, D. M., Bonan, G. B., Flanner, M. G., Kluzek, E., Peter, J., et al.: Technical description of version 4.0 of the Community Land Model (CLM). Boulder: National Center for Atmospheric Research, 2010.

Pagani, M., Arthur, M., and Freeman, K.: Miocene evolution of atmospheric carbondioxide, Paleoceanography, 14, 273–292, doi:10.1029/1999PA900006, 1999.

Pound, M. J., Haywood, A. M., Salzmann, U., & Riding, J. B.: Global vegetation dynamics and latitudinal temperature gradients during the Mid to Late Miocene (15.97–5.33 Ma). Earth-Science Reviews, 112(1–2), 22. https://doi.org/10.1016/j.earscirev.2012.02.005, 2012

Rae, J.W.B., Zhang, Y.G., Liu, X., Foster, G.L., Stoll, H.M., Whiteford, R.D.M.: Atmospheric CO2 over the past 66 Million Years from Marine Archives. Annu. Rev. Earth Planet. Sci, 49, 609-641, 2021.

Reichgelt, T., & West, C. K.: Insights into greener Miocene biomes and globally enhanced terrestrial productivity from fossil leaves. *Evolving Earth*, *3*, 100058, 2025.

Reichgelt, T., Baumgartner, A., Feng, R., Willard, D.A.: Poleward amplification, seasonal rainfall and forest heterogeneity in the Miocene of the eastern USA. Global and Planetary Change 222, 104073, 2023.

Reichgelt, T., Greenwood, D. R., Steinig, S., Conran, J. G., Hutchinson, D. K., Lunt, D. J., ... & Zhu, J.: Plant proxy evidence for high rainfall and productivity in the Eocene of Australia. *Paleoceanography and Paleoclimatology*, *37*(6), e2022PA004418, 2022.

Riahi, K., Van Vuuren, D. P., Kriegler, E., Edmonds, J., O'neill, B. C., Fujimori, S., ... & Tavoni, M.: The Shared Socioeconomic Pathways and their energy, land use, and greenhouse gas emissions implications: An overview. *Global environmental change*, *42*, 153-168, 2017.

Rye, R. O., & Stoffregen, R. E.: Jarosite-water oxygen and hydrogen isotope fractionations; preliminary experimental data. *Economic Geology*, *90*(8), 2336-2342, 1995.

Savin, S.M. & Lee, M.: Isotopic studies of phyllosilicates, in Bailey, S.W., ed., Hydrous phyllosilicates, Reviews in Mineralogy 19: 189-223, 1998.

Schouten, S., Hopmans, E. C., and Sinninghe Damsté, J. S.: The organic geochemistry of glycerol dialkyl glycerol tetraether lipids: A review, Organic Geochemistry, 54, 19-61, doi: 10.1016/j.orggeochem.2012.09.006, 2013.

https://doi.org/10.5194/egusphere-2026-899
Preprint. Discussion started: 24 February 2026

Seager, R., Naik, N., & Vecchi, G. A.: Thermodynamic and dynamic mechanisms for large-scale changes in the hydrological cycle in response to global warming. *Journal of climate*, *23*(17), 4651-4668, 2010.

Seltzer, A. M., Blard, P. H., Sherwood, S. C., & Kageyama, M.: Terrestrial amplification of past, present, and future climate change. *Science Advances*, *9*(6), eadf8119, 2023.

Sheppard, S. M. F., & Gilg, H. A.: Stable isotope geochemistry of clay minerals:"The story of sloppy, sticky, lumpy and tough" Cairns-Smith (1971). *Clay minerals*, *31*(1), 1-24, 1996.

Shevenell, A. E., Kennett, J. P., & Lea, D. W.: Middle Miocene ice sheet dynamics, deep-sea temperatures, and carbon cycling: A Southern Ocean perspective. Geochemistry, Geophysics, Geosystems, 9(2), Q02006. https://doi.org/10.1029/2007GC001736, 2008

Singh, H. K., Bitz, C. M., Donohoe, A., Nusbaumer, J., & Noone, D. C.: A mathematical framework for analysis of water tracers. Part II: Understanding large-scale perturbations in the hydrological cycle due to CO 2 doubling. *Journal of Climate*, *29*(18), 6765-6782, 2016.

Smith, R., P. Jones, B. Briegleb, F. Bryan, G. Danabasoglu, J. Dennis, et al.: The Parallel Ocean Program (POP) Reference Manual, Ocean Component of the Community Climate System Model (CCSM). Tech. Rep., Los Alamos National Laboratory Tech. Rep. LAUR-10-01853, 2010.

Sosdian, S. M., Greenop, R., Hain, M. P., Foster, G. L., Pearson, P. N., & Lear, C. H.: Constraining the evolution of Neogene ocean carbonate chemistry using the boron isotope pH proxy. Earth and Planetary Science Letters, 498, 362–376. https://doi.org/10.1016/j.epsl.2018.06.017, 2018

Spicer, R. A., Yang, J., Spicer, T. E. V., & Farnsworth, A.: Woody dicot leaf traits as a palaeoclimate proxy: 100 years of development and application. Palaeogeography, Palaeoclimatology, Palaeoecology, 562, 110138. https://doi.org/10.1016/j.palaeo.2020.110138, 2021

Steinthorsdottir, M., Coxall, H. K., de Boer, A. M., Huber, M., Barbolini, N., Bradshaw, C. D., et al.: The Miocene: The future of the past. Paleoceanography and Paleoclimatology, 36, e2020PA004037. https://doi.org/10.1029/2020PA004037, 2021

Steinthorsdottir, M., Jardine, P. E., & Rember, W. C.: Near-Future pCO2 during the hot Miocene Climatic Optimum. Paleoceanography and Paleoclimatology, 36, e2020PA003900. https://doi.org/10.1029/2020PA003900, 2020

Sun, Y., Ding, L., Su, B., Stepanek, C., and Ramstein, G.: Simulating surface warming in Earth's three polar regions during the Middle Miocene Climatic Optimum using isotopic and non-isotopic versions of the Community Earth System Model. Palaeogeography, Palaeoclimatology, Palaeoecology, Volume 643,2024,112156,ISSN 0031-0182, https://doi.org/10.1016/j.palaeo.2024.112156, 2024.

Super, J. R., Thomas, E., Pagani, M., Huber, M., O'Brien, C. L., & Hull, P. M.: Miocene evolution of North Atlantic Sea surface temperature. Paleoceanography and Paleoclimatology, 35. https://doi.org/10.1029/2019PA003748, 2020

Taylor, K. E., Crucifix, M., Braconnot, P., Hewitt, C. D., Doutriaux, C., Broccoli, A. J., ... & Webb, M. J.: Estimating shortwave radiative forcing and response in climate models. *Journal of Climate*, *20*(11), 2530-2543, 2007.

Taylor, K. E., Stouffer, R. J., and Meehl, G. A.: An Overview of CMIP5 and the Experiment Design, B. Am. Meteorol. Soc., 93, 485–498, 2012

Tierney, J. E., & Tingley, M. P.: BAYSPLINE: A new calibration for the alkenone paleothermometer. Paleoceanography and Paleoclimatology, 33(3), 281–301, 2018.

https://doi.org/10.5194/egusphere-2026-899
Preprint. Discussion started: 24 February 2026

Tierney, J. E., Haywood, A. M., Feng, R., Bhattacharya, T., & Otto-Bliesner, B. L.: Pliocene warmth consistent with greenhouse gas forcing. *Geophysical Research Letters*, *46*(15), 9136-9144, 2019.

Tierney, J.E. et al.: Past climates inform our future. Science, 370(6517), eaay3701, doi:10.1126/science.aay3701, 2020

Tripati, A. K., Hill, P. S., Eagle, R. A., Mosenfelder, J. L., Tang, J., Schauble, E. A., Eiler, J. M., Zeebe, R. E., Uchikawa, J., Coplen, T. B., Ries, J. B., and Henry, D.: Beyond temperature: Clumped isotope signatures in dissolved inorganic carbon species and the influence of solution chemistry on carbonate mineral composition, Geochim. Cosmochim. Acta, 166, 344–371, https://doi.org/10.1016/j.gca.2015.06.021, 2015.

Uhl, D., Mosbrugger, V., Bruch, A., & Utescher, T.: Reconstructing palaeotemperatures using leaf floras—Case studies for a comparison of leaf margin analysis and the coexistence approach. Review of Palaeobotany and Palynology, 126(1–2), 49–64. https://doi.org/10.1016/s0034-6667(03)00058-7, 2003

Utescher, T., Bruch, A. A., Erdei, B., François, L., Ivanov, D., Jacques, F. M. B., et al.: The coexistence approach—Theoretical background and practical considerations of using plant fossils for climate quantification. Palaeogeography, Palaeoclimatology, Palaeoecology, 410, 58–73. https://doi.org/10.1016/j.palaeo.2014.05.031, 2014

Vincent, E., & Berger, W. H.: Carbon dioxide and polar cooling in the Miocene: The Monterey hypothesis. In The carbon cycle and atmospheric CO2 natural variations Archean to present, 32, 455–468, 1985.

Weijers, J. W. H., Panoto, E., van Bleijswijk, J., Schouten, S., Rijpstra, W. I. C., Balk, M., Stams, A. J. M., and Sinninghe Damsté, J. S.: Constraints on the Biological Source(s) of the Orphan Branched Tetraether Membrane Lipids, Geomicrobiol. J., 26, 402-414, doi: 10.1080/01490450902937293, 2009.

Winnick, M. J., Caves, J. K., & Chamberlain, C. P.: A mechanistic analysis of early Eocene latitudinal gradients of isotopes in precipitation. *Geophysical Research Letters*, *42*(19), 8216-8224, 2015.

Zhang, Y. G., Pagani, M., Liu, Z., Bohaty, S. M., & DeConto, R.: A 40-million-year history of atmospheric CO2. *Philosophical Transactions of the Royal Society A: Mathematical, Physical and Engineering Sciences*, *371*(2001), 20130096, 2013.

Zhu, J., Liu, Z., Brady, E. C., Otto-Bliesner, B. L., Marcott, S. A., Zhang, J., et al.: Investigating the direct meltwater effect in terrestrial oxygen-isotope paleoclimate records using an isotope-enabled Earth system model. Geophysical Research Letters, 44,12,501–12,510. https://doi.org/10.1002/2017GL076253, 2017

Zhu, J., Otto-Bliesner, B. L., Brady, E. C., Poulsen, C. J., Tierney, J. E., Lofverstrom, M., & DiNezio, P.: Assessment of equilibrium climate sensitivity of the Community Earth System Model version 2 through simulation of the Last Glacial Maximum. *Geophysical Research Letters*, *48*(3), e2020GL091220, 2021.

https://doi.org/10.5194/egusphere-2026-899
Preprint. Discussion started: 24 February 2026

Zhu, J., Poulsen, C. J., & Tierney, J. E.: Simulation of Eocene extreme warmth and high climate sensitivity through cloud feedbacks. Science Advances, 5(9), eaax1874. https://doi.org/10.1126/sciadv.aax1874, 2019

Zhu, J., Poulsen, C. J., Otto-Bliesner, B. L., Liu, Z., Brady, E. C., & Noone, D. C.: Simulation of early Eocene water isotopes using an Earth system model and its implication for past climate reconstruction. *Earth and Planetary Science Letters*, *537*, 116164, 2020.